Electronic Supplementary Information

Achilles' heel of iron-based catalysts during oxygen reduction in acidic medium

Chang Hyuck Choi*[a], Hyung-Kyu Lim[b], Min Wook Chung[a], Gajeon Chon[a], Nastaran Ranjbar Sahraie[c], Abdulrahman Altin[d], Moulay-Tahar Sougrati[c], Lorenzo Stievano[c], Hyun Seok Oh[e], Eun Soo Park[e], Fang Luo[f], Peter Strasser[f], Goran Dražić[g], Karl J. J. Mayrhofer[d,h,i], Hyungjun Kim*[b] and Frédéric Jaouen*[c]

[a]School of Materials Science and Engineering, Gwangju Institute of Science and Technology, 61005 Gwangju, Republic of Korea.

[b]Department of Chemistry, Graduate School of EEWS, Korea Advanced Institute of Science and Technology, 34141 Daejeon, Republic of Korea.

[c]Institut Charles Gerhardt Montpellier, UMR 5253, CNRS - Université de Montpellier ENSCM, 34095 Montpellier Cedex 5, France.

[d]Department of Interface Chemistry and Surface Engineering, Max-Planck Institut für Eisenforschung GmbH, Max-Planck-Str. 1, 40237 Düsseldorf, Germany.

[e]Department of Materials Science and Engineering, Seoul National University, 08826 Seoul, Republic of Korea.

[f]Department of Chemistry, Chemical Engineering Division, Technical University Berlin, 10623 Berlin, Germany.

[g]Department of Materials Chemistry, National Institute of Chemistry, Hajdrihova 19, 1001 Ljubljana, Slovenia.

[h]Helmholtz-Institute Erlangen-Nürnberg for Renewable Energy (IEK-11), Forschungszentrum

Jülich, Egerlandstr. 3, 91058 Erlangen, Germany.

[i]Department of Chemical and Biological Engineering, Friedrich-Alexander-Universität Erlangen-Nürnberg, Egerlandstr. 3, 91058 Erlangen, Germany.

*Correspondence to: Chang Hyuck Choi (chchoi@gist.ac.kr), Hyungjun Kim (linus16@kaist.ac.kr) or Frédéric Jaouen (frederic.jaouen@umontpellier.fr)

Experimental Section

Catalyst synthesis and H_2O_2-treatment. FeNC-1 and FeNC-0.5 were prepared from Fe^{II} acetate, 1,10-phenanthroline (phen), and a Zn^{II} zeolitic imidazolate framework (ZIF-8 with formula $ZnN_4C_8H_{12}$, purchased from BASF under trademark Basolite Z1200). One gram of a catalyst precursor containing 1.0 or 0.5 wt% Fe with a mass-ratio phen/ZIF-8 of 20/80 was prepared by dry ball-milling. The milling was carried out in a ZrO_2 crucible with 100 ZrO_2 balls of 5 mm diameter using a planetary ball-miller (FRITSCH Pulverisette 7 Premium) for 4 cycles of 30 min at 400 rpm. The resulting catalyst precursors were then pyrolyzed at 1050 °C in Ar for 1 h, leading to FeNC-1 and FeNC-0.5. The Fe content in the catalysts after pyrolysis was measured with inductively-coupled plasma-atomic emission spectroscopy, and found to be 3.0 and 1.5 wt%, respectively. This three-fold increase relative to the Fe content in the catalyst precursors is typical for such catalysts, and is due to ZIF-8 and phenanthroline losing about 66 % of their mass during pyrolysis while no Fe-containing volatile products form. The H_2O_2-treatment was performed in a 0.1 M $HClO_4$ or 0.1 M KOH solution containing 5 wt% H_2O_2, referred to as the oxidizing solution. It was prepared from concentrated $HClO_4$ (70 %, Aldrich), H_2O_2 (30 wt%, Aldrich) and ultrapure water (18 MΩ, Millipore). For physical characterization purposes, the H_2O_2-treatment was performed with 0.05 g of Fe-N-C catalyst dispersed into 300 mL of the oxidizing solution at 20, 50 or 70 °C. After 2 h, the catalyst powder was collected by filtration, washed with 1 L ultrapure water and dried at 80 °C. For electrochemical characterization purposes, the FeNC-1 based catalytic layer (loading 800 μg cm^{-2}) deposited on the glassy carbon tip (3 mm diameter) was immersed in 100 mL of the oxidizing solution for 2 h, a method similar to that previously employed,[1] with the electrode rotated at 2000 rpm to remove O_2-bubbles formed from H_2O_2 disproportionation and the

electrode potential was either set at 0.5 V_{RHE} or left at open-circuit potential (OCP). The OCP value of FeNC-1 was *ca.* 0.84 V_{RHE} in 0.1 M $HClO_4$ and *ca.* 0.94 V_{RHE} in 0.1 M KOH.

Physico-chemical characterizations. Inductively coupled plasma-atomic emission spectrometry analysis (ICP-AES) was carried out using a POLYSCAN 61E (Hewlett-Packard).

Electron paramagnetic resonance (EPR) was performed using a Bruker EMX/Plus spectrometer equipped with a dual mode cavity (ER 4116DM). The experimental conditions are as follows: 9.64 GHz microwave frequency, 10 G modulation amplitude, 100 kHz modulation frequency, 0.94 mW microwave power and 298 K temperature. For each spectrum 10 scans were accumulated. EPR aliquot samples were prepared as follows. A mass of 1.8 mg FeNC-0.5 catalyst was dispersed in either 0.1 M $HClO_4$ or 0.1 M KOH solution. After 30 min of sonication, the desired amounts of 5,5-Dimethyl-1-pyrroline N-oxide (DMPO; >98%, Aldrich) and hydrogen peroxide were sequentially added to reach the concentrations of 0.4 M and 0.5 wt%, respectively. The resulting total volume of the solution was 0.5 mL. After 5 min of reaction, the solution was filtered (syringe polypropylene filter, 0.2 μm, Whatman) to separate the catalyst powder from the liquid aliquot that was subsequently examined with EPR.

X-ray absorption spectroscopy (XAS) at the Fe K-edge was measured in transmission mode at Pohang Accelerator Laboratory (7D-XAFS beamline). A mass of 0.1 g catalyst was mounted in a sample holder ($w \times l \times d$=3×8×2 mm^3). The XAS energy scale was calibrated using a Fe foil before and after the measurement to verify the lack of or correct for any energy shift during data acquisition. For extended X-ray absorption fine structure (EXAFS) analysis, Artemis implemented in Demeter program package (0.9.23) was utilized after the data processing in Athena.[2] EXAFS amplitudes and phase shifts were calculated by FEFF7. The many body attenuation factor (S_0^2) was determined as 0.82 from the fit of the EXAFS of reference

materials. Interatomic distances (R) and the Debye-Waller factors were calculated for all paths included in the fits. ^{57}Fe Mössbauer spectra were measured with a source of ^{57}Co-Rh. The measurements were performed with both the source and the absorber at room temperature. The spectrometer was operated with a triangular velocity waveform, and a NaI scintillation detector was used for detecting the γ-rays. Velocity calibration was performed with an α-Fe foil, to which all isomer shifts are referred. The broadened quadrupole components of the Mössbauer spectra were analysed in Fig. S6 by assuming Gaussian distributions of the electric quadrupole interaction. Three independent Gaussian distribution components were necessary to fit coherently the whole series of collected spectra. CO pulse chemisorption was performed with a Thermoscientific TPD/R/O 1110 instrument under 20 mL min^{-1} He flow. Typically, 100-150 mg catalyst was cleaned by heating at 20 °C min^{-1} to 600 °C (hold time 15 min) in He, and then cooled down to room temperature. CO pulse chemisorption was then carried out at 193 K with the sample holder immersed in a dry ice and acetone mix. Six CO pulses (0.338 mL) were carried out at 25 min interval. The adsorbed CO amount was quantified from the difference between the area below peaks No. 4-6 and that below peaks No. 1-3. From the adsorbed CO amount and the bulk Fe content measured by ICP, the relative amount of Fe that is on the surface and interacts with CO was calculated, assuming one CO molecule binds per FeN_xC_y moiety. The relative amount of surface Fe probed by CO chemisorption may underestimate the true amount of surface Fe, if some surface FeN_xC_y moieties do not bind CO. N_2 adsorption-desorption isotherms were measured using a BEL-sorp-max (BEL Japan) volumetric analyzer at 77 K. Before each measurement, the sample was degassed at 200 °C for 4 h. The specific areas were determined in the P/P_0 range of 0.05-0.15 using the Brunauer-Emmett-Teller (BET) equation.

Probe Cs-corrected scanning transmission electron microscope Jeol ARM 200 F, equipped with a cold field emission electron source, was used for imaging atomically-dispersed FeN_xC_y moieties, and possibly binuclear $Fe_2N_xC_y$ moieties, in FeNC-1. To minimize the beam damage, 80 keV and low beam current were used. High-angle annular dark-field (HAADF) images were obtained using 68-180 mrad collection half-angles at 24 mrad probe convergence semi-angle. Images were filtered with non-linear filter which is a combination of low-pass and Wiener filters.[3] The presence of iron and nitrogen was confirmed with Gatan Quantum ER dual Electron Energy-loss Spectroscopy (EELS) system.

X-ray photoelectron spectroscopy (XPS) and ultraviolet photoelectron spectroscopy (UPS) data acquisition were carried out using a Sigma Probe (Thermo VG Scientific) equipped with a microfocused monochromator X-ray source. The XPS data were analysed using the XPSPEAK41 software with ±0.1 eV deviation in binding energy. The binding energies used for deconvoluting the XPS-N_{1s} spectra were 398.5 eV for pyridinic-N, 400.1 eV for pyrrolic-N, 401.1 eV for graphitic-N and 403.7 eV for pyridinic-oxide, respectively.[4] The binding energies used for deconvoluting the XPS-O_{1s} spectra were 531.2 eV for C=O and 533.0 eV for C-O, respectively.[5,6] UPS data were analysed with He I radiation. The work function (WF) values were derived from the following equation

$$\mathrm{WF} = h\nu - |E_{\mathrm{sec}} - E_{\mathrm{Fermi}}| \quad (1)$$

where $h\nu$ is the 21.2 eV radiation energy of He I source, E_{sec} is the onset of the secondary emission, and E_{Fermi} is the Fermi edge level. The potential of zero charge, E_{PZC}, was measured using a VPM3 potentiostat (BioLogic) installed with a function of staircase potentiostatic electrochemical impedance spectroscopy. The measurements were performed in a 2 mM NaF electrolyte from –1.5 to 0.5 $V_{Ag/AgCl}$ at 100 mHz frequency and with a 10 mV potential

amplitude. E_{PZC} was determined as the potential at which the electrochemical double layer shows a minimum capacitance. Basicity of the catalytic surface was measured by dispersing 40 mg of FeNC-1 or H_2O_2-treated FeNC-1 catalysts in 20 mL of an aqueous solution of initial pH (pH_i) 6 prepared from 0.1 M H_2SO_4 and 0.1 M KOH solutions, continuously saturated with bubbling N_2 to prevent acidification from airborne CO_2.[7] The final pH after equilibration was recorded once the pH-meter indicated a stable value. For Fe-N-C catalysts, we previously reported that the entire curve $pH_f = f(pH_i)$, with pH_i values ranging from 1 to 13, shows a plateau of pH_f values, at near-neutral pH_i values, and discussed that the plateau of pH_f is a measure of the surface basicity.[7,8] For comparing the basicity of H_2O_2-treated samples relative to pristine FeNC-1, we therefore used the pH variation $\Delta pH_f = pH_f$ (H_2O_2-treated FeNC-1) – pH_f (pristine FeNC-1).

Electrochemical characterizations. The electrochemical properties were studied with a modulated speed rotator (RRDE-3A, ALS) in a three-electrode Teflon cell equipped with a graphite rod as a counter electrode and a saturated Ag/AgCl as a reference electrode (RE-1A for acidic medium and RE-16 for alkaline medium, EC-Frontier). 0.1 M $HClO_4$ and 0.1 M KOH solutions were used as acidic and alkaline electrolytes, respectively. They were prepared from concentrated $HClO_4$ (70 %, Aldrich) and KOH pellet (90 %, Aldrich) with ultrapure water (18 MΩ, Millipore). Before any electrochemical measurements, the Ag/AgCl reference electrodes were calibrated against a Pt electrode in H_2-saturated electrolyte to correctly convert potentials to the reversible hydrogen electrode (RHE) scale. ORR activity was investigated at a loading of 800 μg_{FeNC} cm^{-2} (*ca.* 25 μg_{Fe} cm^{-2} for FeNC-1). The catalyst ink was prepared by dispersing 10 mg catalyst in 884 µL aliquot (804 µL water and 80 µL of 5 wt% Nafion solution). The working electrode was prepared by pipetting 5 µL of catalyst ink onto the glassy

carbon disk (0.071 cm^2) of the rotating disk electrode (011169, ALS), which was then left to dry at room temperature. For comparison, a 46 wt% Pt/C (TEC10E50E, Tanaka) electrode was prepared with 20 μg_{Pt} cm^{-2} Pt loading. The ORR polarization curves were recorded with a scan rate of 10 mV s^{-1} and a rotation speed of 900 rpm in an O_2-saturated electrolyte. ORR Faradaic currents were obtained after subtraction of the polarization curves measured identically but in Ar-saturated electrolyte. Onset potential was defined as the potential at which 0.1 mA cm^{-2} current density is reached.

Rotating ring disk electrode (RRDE) analysis was carried out using a RRDE electrode (012613, ALS) composed with Pt ring and glassy carbon disk electrodes. During the measurement, the Pt ring disk was set at 1.2 V_{RHE} and the electrode was rotated at 900 rpm. H_2O_2 selectivity was calculated using the following equation

$$H_2O_2\ (\%) = 200 \times I_R/N\ /\ (I_D + I_R/N) \qquad (2)$$

where I_R is the ring current, I_D is the disk current and N is the collection efficiency (0.32, as determined by $Fe^{2+/3+}$ redox calibration).

All electrochemical experiments on the ORR activity and selectivity on FeNC-1, peroxide-treated FeNC-1 and electrochemically-reduced peroxide-treated FeNC-1 were carried out at least two times for reproducibility assessment. The reproducibility error was *ca*. ±10 % on the ORR activity (relative to the average activity at 0.8 V_{RHE}, acid, or 0.9 V_{RHE}, alkaline) and *ca.* ±2 % on the selectivity (absolute variation of % peroxide detected during RRDE at 0.5 V_{RHE}).

Electrochemical reduction of H_2O_2-treated FeNC-1 and FeNC-0.5. Electrochemical reduction of the carbon surface on FeNC-1-20, -50 and -70 and FeNC-0.5-70 was carried out by cyclic voltammetry (CV) in an Ar-saturated 0.5 M NaCl electrolyte, a method similar to that employed for electrochemical reduction of graphene oxide to graphene.[9,10] 100 cycles were

progressed between 0 and −1.6 $V_{Ag/AgCl}$ with a scan rate of 100 mV s^{-1}. The lower potential limit was selected to avoid significant hydrogen evolution at even lower potential, leading to active-layer detachment.

Computational methods. We performed first-principle DFT calculations coupled with the Poisson-Boltzmann (PB) implicit solvation effect on models for active sites with different environments as shown in Fig. S8a. We used the Vienna Ab-initio Simulation Package (VASP),[11] with the exchange-correlation function of revised Perdew-Burke-Ernzerhof (RPBE).[12] The electron-ion interaction was considered in the form of the projector-augmented-wave (PAW) method with a plane wave up to energy of 600 eV. The active site models combined with a 20 Å vacuum layer along the z-axis were fully minimized under a gamma centered k-point grid of (4×4×1). A dipole correction was applied to all calculation cases to avoid unwanted electrostatic interaction between periodic images along the z-direction. To calculate the solvation energy, the PB implicit solvation model, which is implemented in the VASP program,[13] was used under a dielectric constant ε = 80 for water (we neglect the cavitation energy contribution). We also calculated the vibrational internal energy and entropy terms for adsorbate molecules by taking account partial Hessian analysis. The partial density of states (PDOS) data was calculated with the conditions of tetrahedron method with Blöchl corrections and manipulated with p4vasp software.

Supplementary Figures and Table

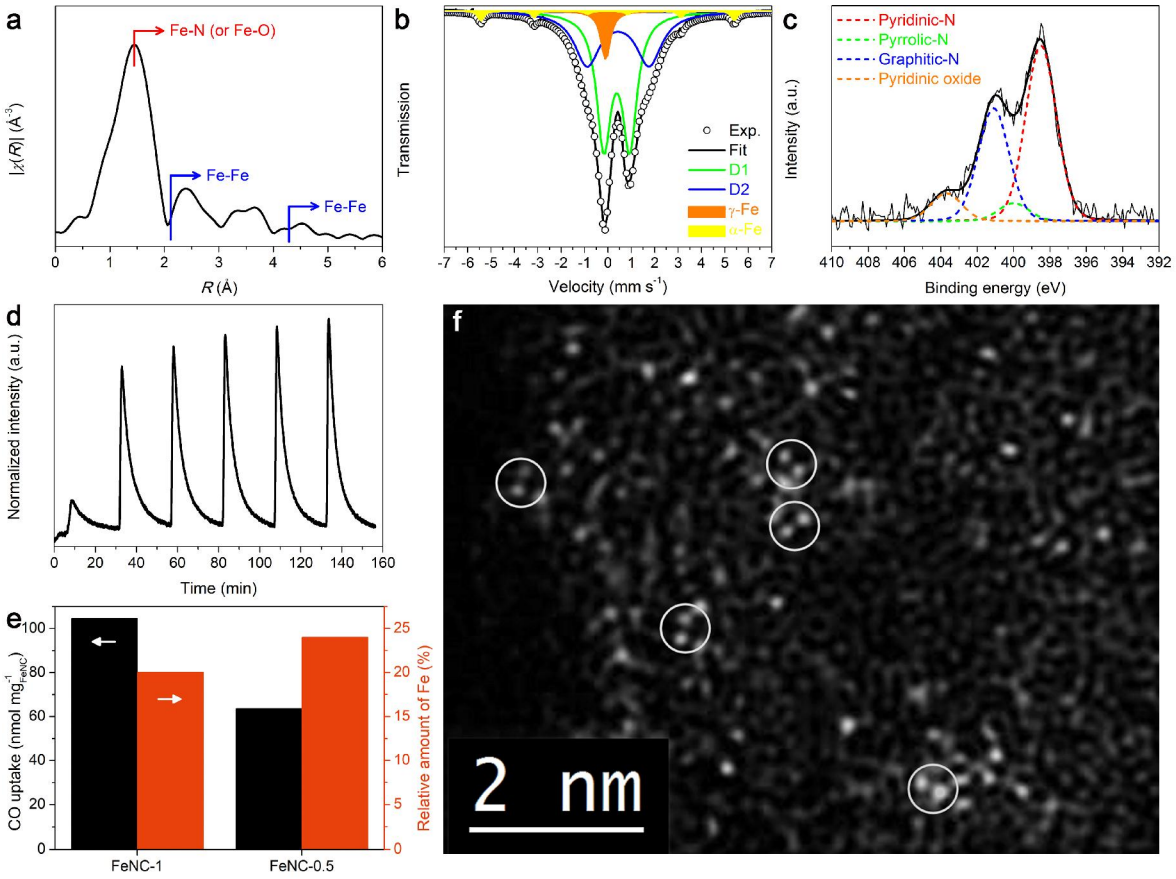

Fig. S1 Physico-chemical characterizations of FeNC-1. (a) k^2-weighted Fourier transforms of Fe K-edge EXAFS on FeNC-1. The analysis showed a predominant presence of Fe-N (or Fe-O) coordination ($CN_{Fe\text{-}N} = 4$ and $CN_{Fe\text{-}O} = 1$) and a minor presence of Fe-Fe coordination ($CN_{Fe\text{-}Fe} = 0.6$). (b) Mössbauer spectrum of FeNC-1. D1 and D2 were assigned to FeN_xC_y moieties with low and medium spins, respectively. (c) XPS-N_{1s} spectrum of FeNC-1. The signal was deconvoluted with pyridinic-N, pyrrolic-N, graphitic-N and pyridinic-oxide peaks. (d) Carbon monoxide pulse-chemisorption profiles of FeNC-1, measured at 193 K. (e) Absolute CO uptake and relative Fe amount located on the surface for FeNC-1 and FeNC-0.5, comprising bulk Fe contents of 3.0 and 1.5 wt%, respectively. (f) Filtered HAADF-STEM image of FeNC-1 (scale bar = 2 nm). The image shows the disordered nature of the carbon surface with many defects

and non-hexagonal rings of light atoms, as well as atomically-dispersed iron atoms. Pairs of iron atoms are visible with Fe-Fe distances of 2.5 ± 0.1 Å (white circles), commensurate with the expected Fe-Fe distance in binuclear $Fe_2N_5C_y$ sites.[14,15] The present top-view image can however not confirm if Fe atoms of such apparent pairs are in a same or in different graphene sheets.

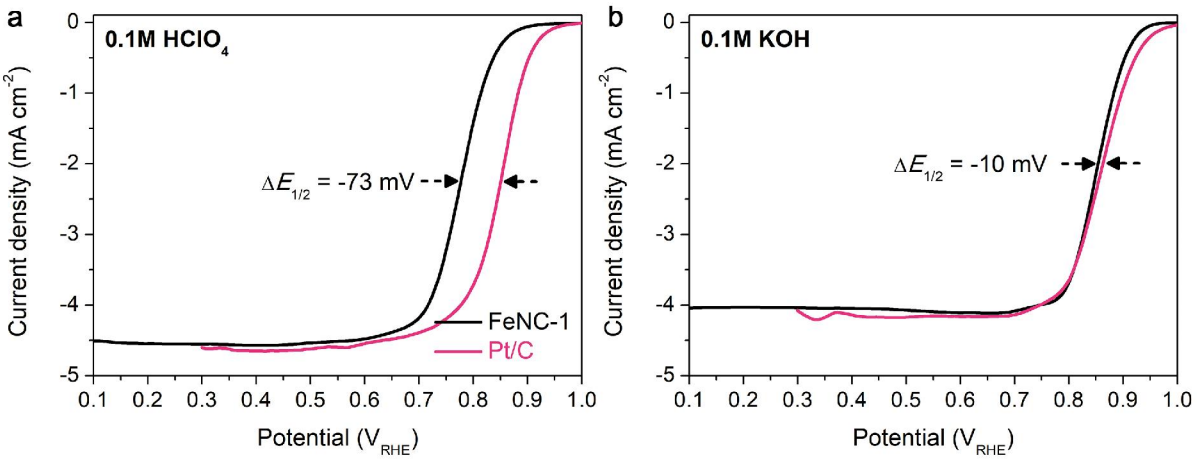

Fig. S2 ORR activity of pristine FeNC-1 catalyst. (a and b) ORR polarization curves of FeNC-1 measured at 900 rpm in (a) O_2-saturated 0.1 M $HClO_4$ and (b) O_2-saturated 0.1 M KOH. The curve for Pt/C was also measured for comparison. Catalyst loadings of FeNC-1 and Pt/C were 800 μg_{FeNC-1} cm^{-2} and 20 μg_{Pt} cm^{-2}, respectively.

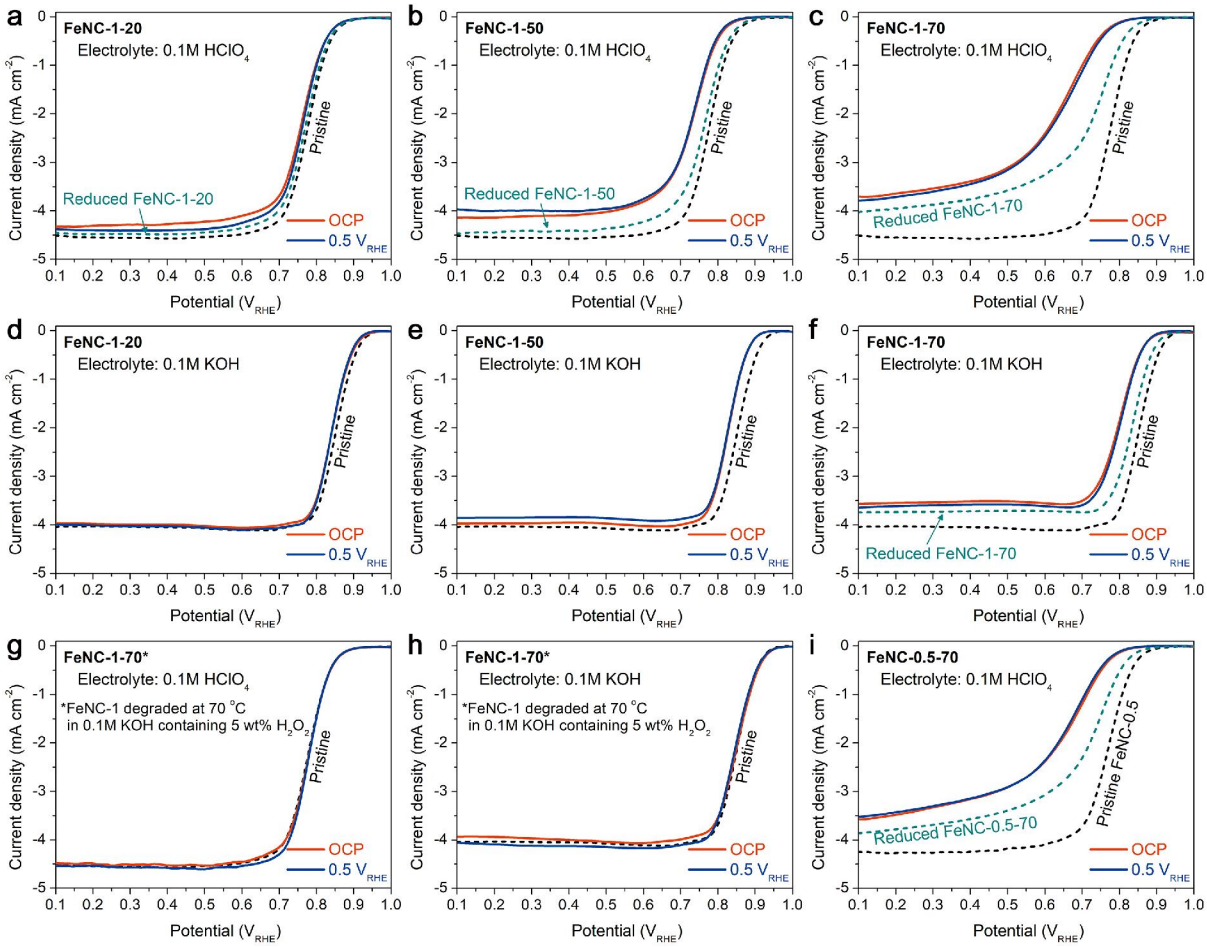

Fig. S3 ORR activity decrease following acidic H_2O_2-treatment and unmodified activity following alkaline H_2O_2-treatment. ORR polarization curves before and after acidic H_2O_2-treatment, measured in (a-c) O_2-saturated 0.1 M $HClO_4$ and (d-f) O_2-saturated 0.1 M KOH. The H_2O_2-treatment was carried out at (a and d) 20, (b and e) 50 or (c and f) 70 ºC in 5 wt% H_2O_2 in 0.1 M $HClO_4$, with the potential fixed either at 0.5 V_{RHE} or open circuit potential (*ca.* 0.84 V_{RHE}). (g and h) ORR polarization curves before and after alkaline H_2O_2-treatment, measured in (g) O_2-saturated 0.1 M $HClO_4$ and (h) O_2-saturated 0.1 M KOH. The H_2O_2-treatment was carried out at 70 ºC in 5 wt% H_2O_2 in 0.1 M KOH, with the electrode potential fixed either at 0.5 V_{RHE} or open circuit potential (*ca.* 0.94 V_{RHE}). (i) ORR polarization curves of FeNC-0.5 before and after acidic H_2O_2-treatment at 70 ºC, measured in O_2-saturated 0.1 M

$HClO_4$. FeNC-0.5 was prepared identically to FeNC-1, except for the halved Fe precursor content, resulting in 100 % Fe being present as FeN_xC_y moieties after pyrolysis.[7] FeNC-0.5 and FeNC-1 respond similarly to H_2O_2-treatment (compare figures i and c). Polarization curves for FeNC-1-70 and FeNC-0.5-70 after electrochemical reduction in 0.5 M NaCl are also shown in (c, f and i) (green dotted curve). The polarization curve for pristine FeNC-1 is shown in all graphs (black dotted curve).

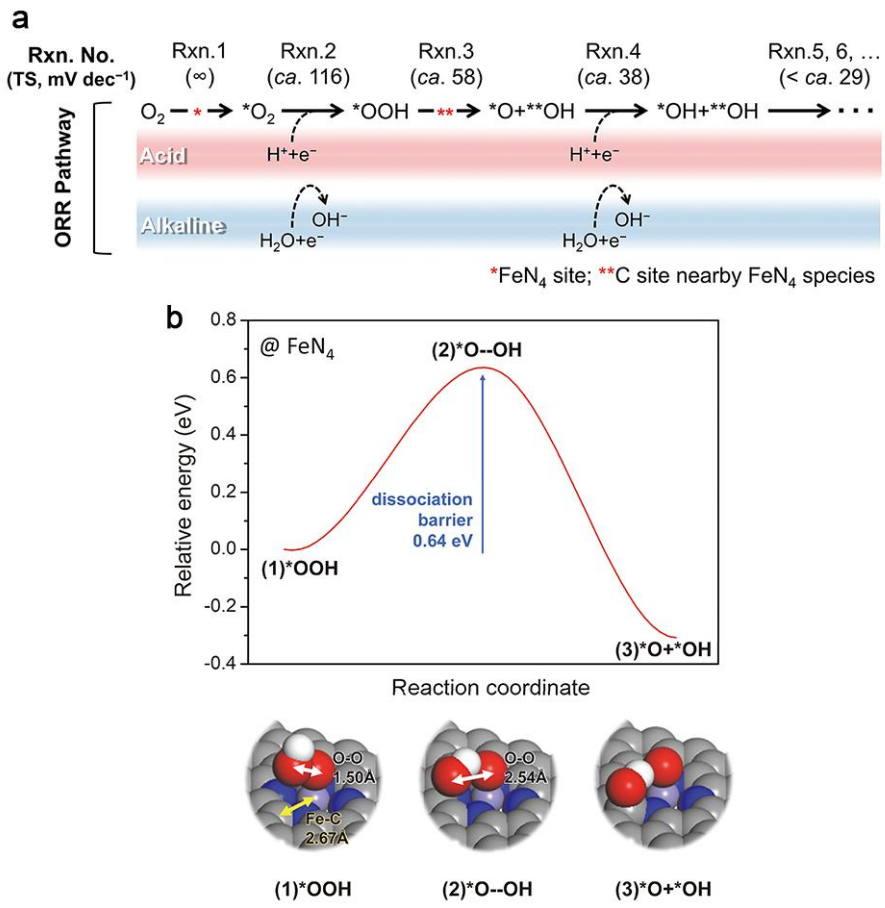

Fig. S4 ORR pathway and Tafel slope (TS). (a) Direct 4e$^-$ ORR mechanism of Fe-N-C catalysts having two adsorption sites (FeN_4 site and C site nearby the FeN_4 moiety).[16] The TS-values were calculated applying TS = $RT\ln10/\alpha F$, where R, T, α and F are the gas constant, temperature, charge-transfer coefficient (a composite term derived from the overall multielectronic reaction and the RDS position in the sequence of elementary steps[17]) and Faraday constant, respectively. TS-values are predicted from first-principles to be *ca.* 116 and 58 mV dec^{-1} when the first-electron transfer step (Rxn. 2) and the consecutive dissociation step (Rxn. 3) are the RDS, respectively. Upon extensively weakened O_2-binding (highly oxidized surface), the first-electron transfer could become the RDS. The steps after the second-electron transfer (Rxn. 4) are not shown since they are not rate-determining (the predicted TS-value would otherwise be < *ca.* 29 mV dec^{-1}, much lower than experimental values of 63-110 mV

dec^{-1} in pH 1). (b) Based on our DFT calculation of the RDS (*OOH dissociation, Rxn. 3) on Fe-N-C catalysts, the distance between a central Fe ion and the nearest carbon atom is 2.67 Å (comparable to the Pt-Pt distance of 2.8 Å on the Pt(111) surface[18]), where O-O bond dissociation can occur with a moderate activation energy barrier of 0.64 eV.

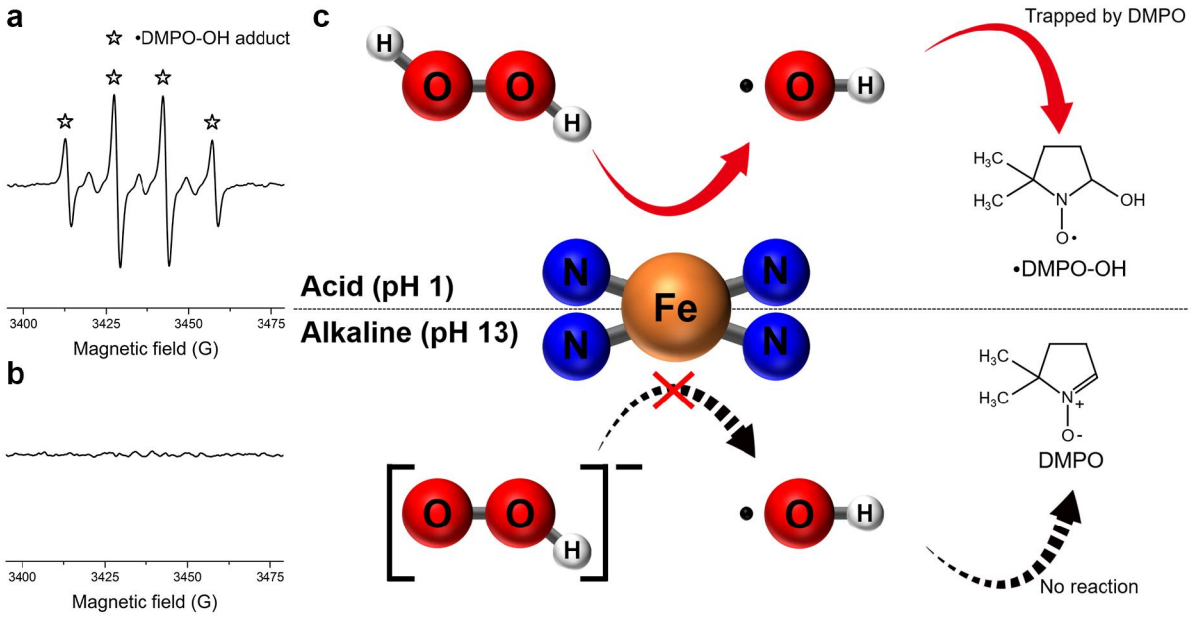

Fig. S5 Spin-trap experiment revealing the formation of ROS during peroxide treatment of Fe-N-C in acidic conditions. (a and b) EPR spectra of filtered solution aliquots after 5 min H_2O_2-treatment at room temperature of FeNC-0.5 in (a) 0.1 M $HClO_4$ or (b) 0.1 M KOH electrolytes. The main quartet signal from ·DMPO-OH was indicated by a star symbol. (c) Scheme of EPR measurement representing the formation of ·DMPO-OH spin adduct in acidic but not in alkaline electrolyte.

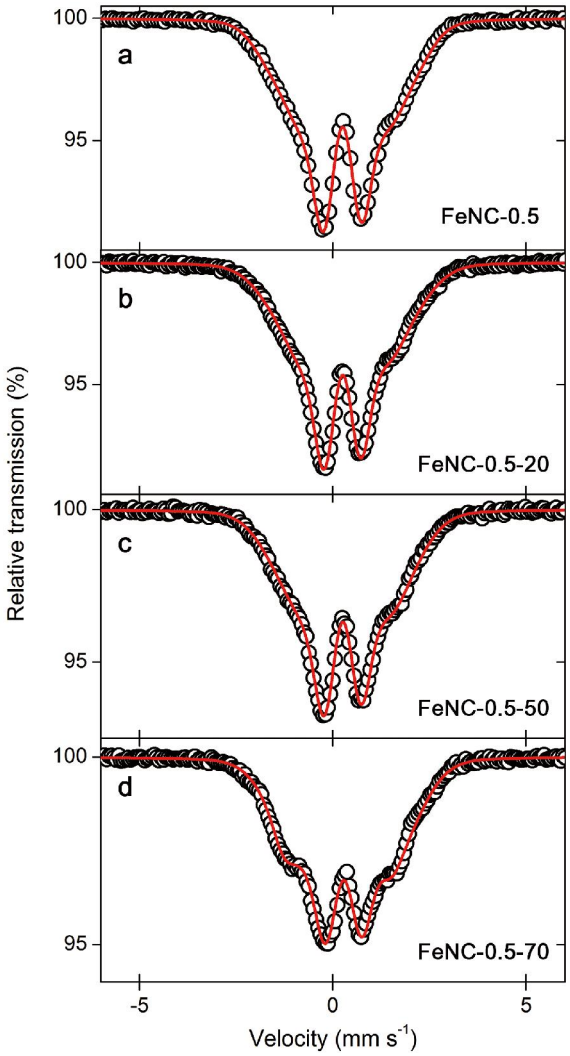

Fig. S6 Room temperature ^{57}Fe Mössbauer spectra of FeNC-0.5 before and after acidic H_2O_2-treatment. (a) Pristine FeNC-0.5, and after treatment in 5 wt% H_2O_2 in 0.1 M $HClO_4$ at (b) 20 °C, (c) 50 °C and (d) 70 °C. The fitting (red curves) was carried out with three Gaussian distributions of the electric quadrupole interaction. The analysis was performed on FeNC-0.5 (halved Fe content relative to FeNC-1) to avoid the singlet (γ-Fe) and sextet (α-Fe), both present in pristine FeNC-1 (Fig. S1b), and that would have impeded the QS-distribution analysis of the subtle changes occurring to the doublet components.

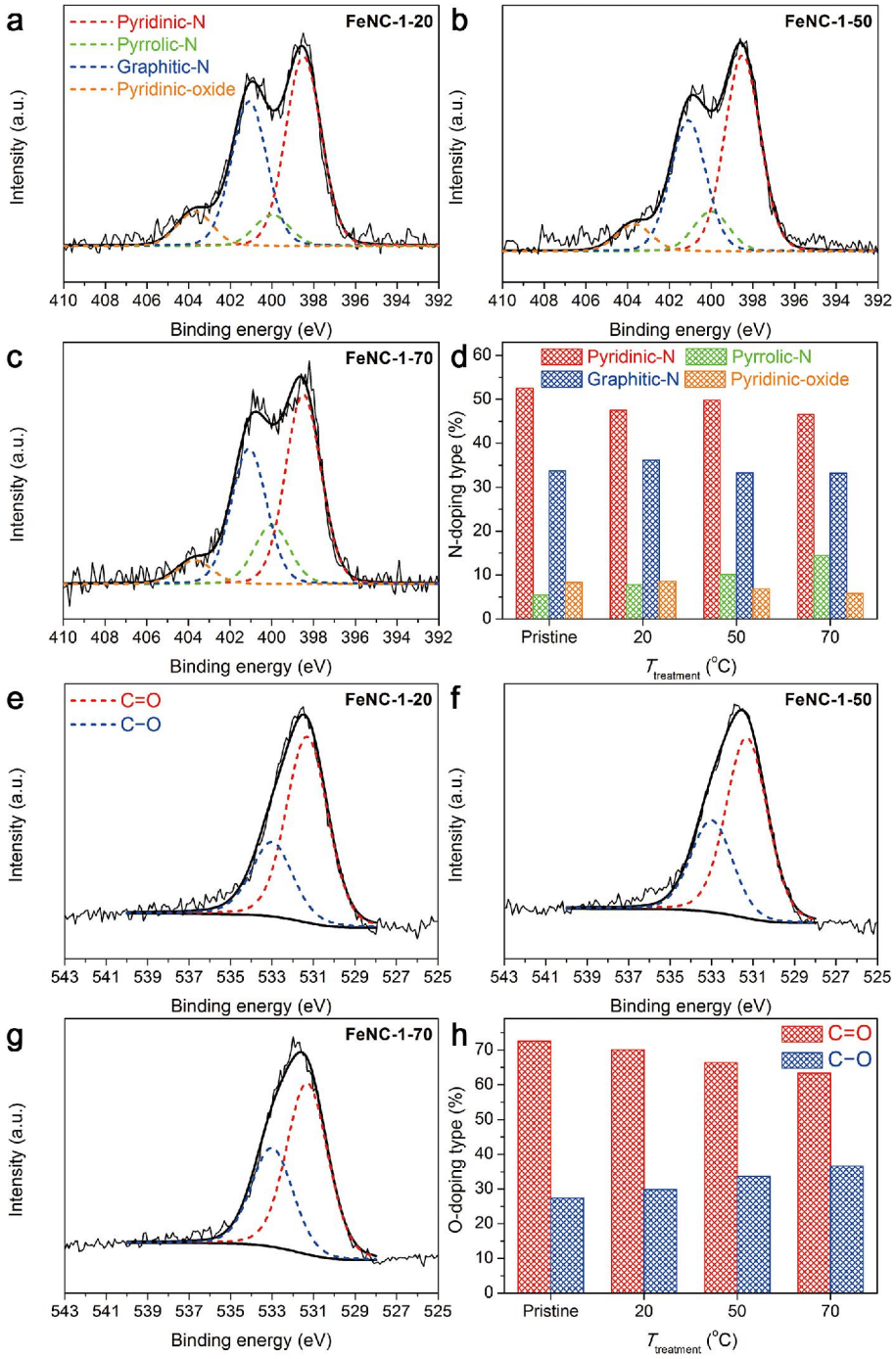

Fig. S7 XPS analyses of FeNC-1 after acidic H_2O_2-treatments. (a-c) XPS-N_{1s} signal and fitting results of FeNC-1 before and after treatment in 5 wt% H_2O_2 in 0.1 M $HClO_4$ at (a) 20 °C, (b) 50 °C and (c) 70 °C. The fitting was carried out with pyridinic-N (398.5 eV, red), pyrrolic-N (400.1 eV, green), graphitic-N (401.1 eV, blue) and pyridinic-oxide (403.7 eV, orange) peaks.[4]

(d) Ratio of N-doping types before and after acidic H_2O_2-treatment. (e-g) XPS-O_{1s} signal and fitting results of FeNC-1 before and after H_2O_2-treatment at (e) 20 °C, (f) 50 °C and (g) 70 °C. The fitting was carried out with C=O (531.2 eV; carbonyl and carboxyl) and C-O (533.0 eV; epoxy and hydroxyl) peaks.[5,6] (h) Ratio of O-doping types before and after acidic H_2O_2-treatment.

a

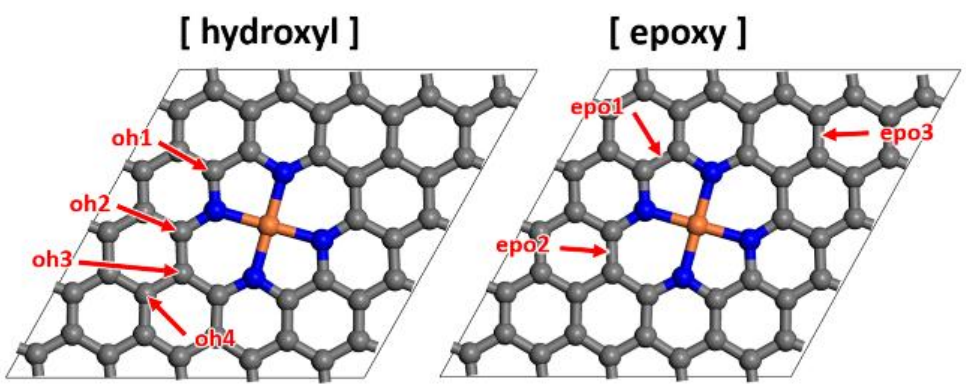

b

	Relative stability (eV)	Boltzmann weight factor @ 300K	*O_2 (eV)	*OOH (eV)	*O (eV)	*OH (eV)
Bare FeN_4	-	-	-0.59	-1.37	-4.09	-2.59
oh1	0.00	0.99	-0.54	-1.33	(-4.15)	(-2.80)
oh2	0.11	0.01	-0.59	-1.17	(-4.20)	(-2.87)
oh3	0.44	0.00	(-0.77)	(-1.68)	(-4.34)	(-2.89)
oh4	0.35	0.00	-0.50	-1.30	-4.02	-2.48
oh1 + oh1'	0.00	1.00	-0.46	-1.26	(-4.16)	(-2.60)
oh2 + oh2'	0.26	0.00	-0.50	(-1.48)	(-4.27)	(-2.99)
oh3 + oh3'	0.74	0.00	(-0.86)	(-1.78)	(-4.49)	(-2.82)
oh4 + oh4'	0.76	0.00	-0.43	-1.28	-4.00	-2.44
epo1	0.00	1.00	-0.30	-1.07	-3.72	-2.26
epo2	0.22	0.00	-0.58	-1.35	-3.99	-2.16
epo3	0.43	0.00	-0.49	-1.33	-4.04	-2.55
epo1 + epo1'	0.00	1.00	0.33	-0.43	-3.22	-1.99
epo2 + epo2'	0.34	0.00	-0.49	-1.30	-3.82	-2.16
epo3 + epo3'	0.89	0.00	-0.44	-1.30	-3.99	-2.51

Fig. S8. (a) Atomistic model of FeN_4 active sites covalently integrated in graphene sheets that was utilized for periodic DFT calculations and the considered oxidation sites for hydroxyl group (oh1 to oh4) and epoxy group (epo1 to epo3). (b) DFT Table reporting from left to right: The relative stability of ensemble of atoms for the same number and kind of oxygen functional groups, the Boltzmann weight factor (derived from the relative stability values) and the binding energies of reaction intermediates at the Fe center for FeN_4 integrated in the considered models of oxidized graphene surfaces. By convention, more negative values mean stronger binding, and second oxidation sites noted with a single quote stand for centrosymmetric sites relative to

the atomic Fe site shown in panel (a). Values in brackets indicate enhanced binding energies for the oxidized case with respect to the bare surface (no oxygen groups on the carbon surface). Here, DFT results show that all epoxy-oxidation configurations weaken the oxophilicity of the Fe center as compared to the bare Fe center. Graphene oxidation by hydroxyl groups also weakens the binding energy of O_2 and OOH on FeN_4 compared to that on the bare Fe center, except for the oh3 site. However, both epoxy and hydroxyl groups energetically strongly prefer to be located at the epo1 and oh1 sites near the FeN_4 active site, respectively (which are quantified to represent >99% using the Boltzmann weight factors). The hydroxyl groups at the first shell (oh1 to oh3) are found to enhance the binding energy of O and OH, which is ascribed to the additional hydrogen bond between the hydroxyl group and the adsorbate; however, it is noted that the key activity descriptor of ORR activity is the O_2 binding energy, which shows a decreasing tendency after all energetically-stable oxidation events considered here.

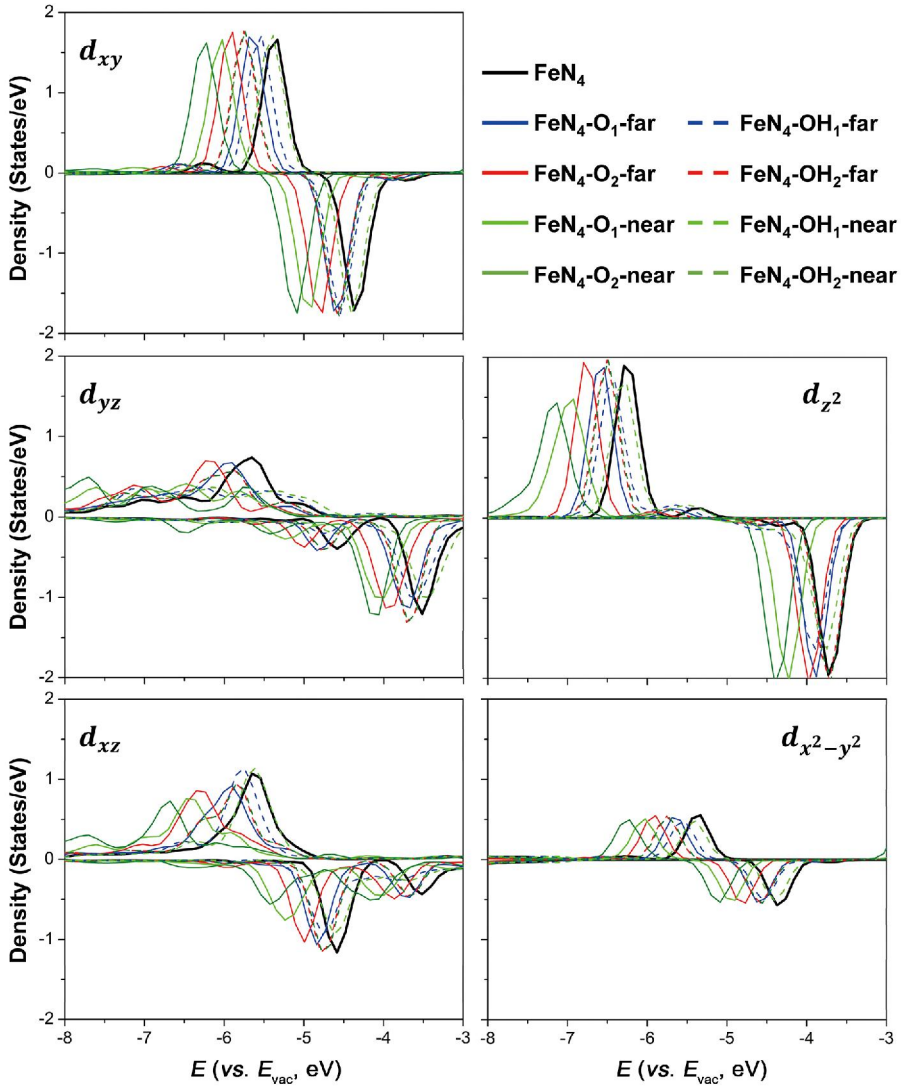

Fig. S9 Fe *d*-orbital locations aligned with respect to the vacuum level (E_{vac}). Energy eigenvalues of Fe *d*-orbitals are blue-shifted as the oxygen-functional groups are introduced into the carbon support. This decreases the hardness and thereby the binding strength of oxygen reaction intermediates to the Fe-center, *i.e.* oxophilicity.

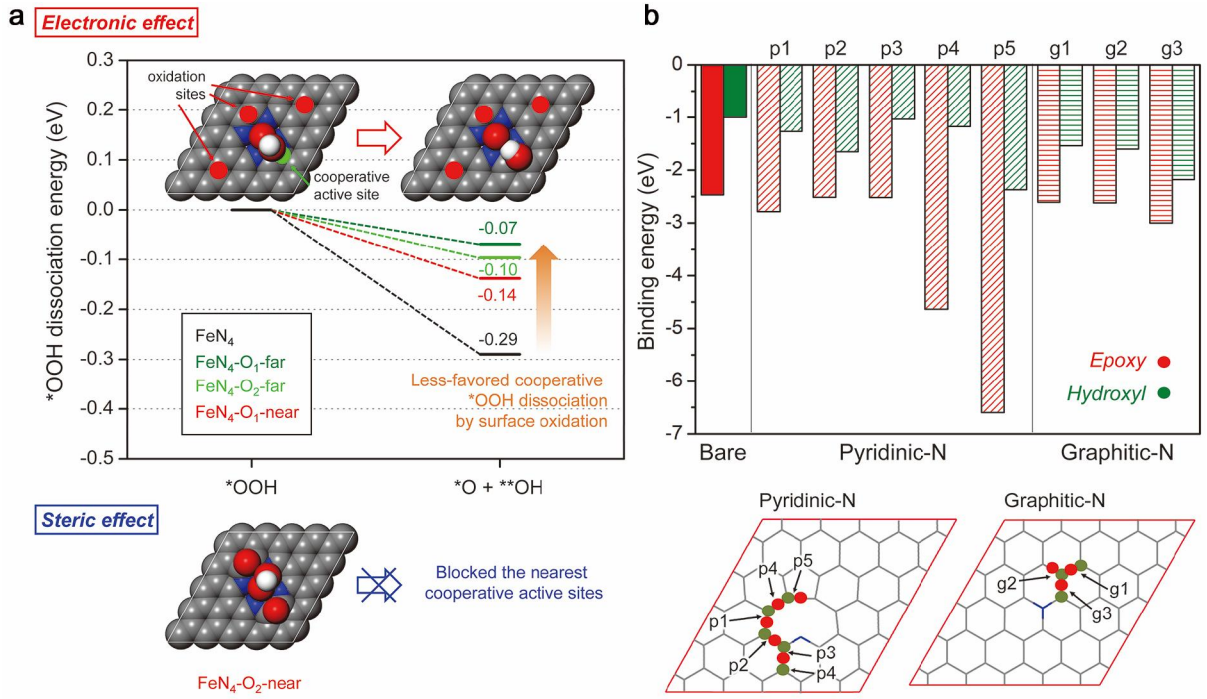

Fig. S10 Retardation of *OOH dissociation pathway by surface oxidation of carbon and enhanced oxygen affinity near N-doped sites. (a) The *OOH dissociation process becomes less favored due to electronic and steric effects as epoxy groups are introduced onto the graphene support near the FeN_4 center, and especially at the nearest carbon center. (b) The calculated binding energies of oxygen-groups to carbon sites situated nearby N-groups (a more negative value means a stronger binding). Compared to the pristine graphene surface showing binding strengths of 2.46 and 0.99 eV for O and OH, respectively, the carbon sites at the five-membered ring near the pyridinic-N site show enhanced binding strength, up to 6.59 and 2.37 eV for O and OH (at p5 site), respectively.

Table S1 Mössbauer and EXAFS fitting results of FeNC-1.

	Component	Relative adsorption area (%)	Relative Fe content (%)	IS[a] (mm s^{-1})	QS[b] (mm s^{-1})	LW[c] (mm s^{-1})
Mössbauer fitting (FeNC-1)	$Fe^{II}N_4$/C-LS (D1)	58	62	0.38	1.10	0.78
	$Fe^{II}N_4$/C-MS (D2)	34	33	0.43	2.65	1.45
	α-Fe (Sextet 1)	3	2	−0.02	–	0.35
	γ-Fe (Singlet)	5	3	−0.10	–	0.42
	Catalyst	Shell	CN[e]	R (Å)[f]	$\Delta\sigma^2$ ($Å^2$)[g]	R-factor
EXAFS fitting[d]	FeNC-1	Fe-N[h]	4	1.97(1)	0.007(2)	0.0019
		Fe-O[h]	1	2.09(2)	0.003(2)	
		Fe-Fe[i]	0.6(3)	2.49(1)	0.011(8)	
	FeNC-1-20	Fe-N	4	1.98(2)	0.007(1)	0.0075
		Fe-O	1	2.10(4)	0.003(2)	
		Fe-Fe	0.5(3)	2.49(2)	0.009(8)	
	FeNC-1-50	Fe-N	4	1.98(2)	0.007(2)	0.0087
		Fe-O	1	2.08(4)	0.003(2)	
		Fe-Fe	0.6(5)	2.49(2)	0.010(8)	
	FeNC-1-70	Fe-N	4	1.98(2)	0.007(2)	0.0087
		Fe-O	1	2.10(5)	0.003(2)	
		Fe-Fe	0.5(4)	2.49(3)	0.008(8)	

[a] Isomer shift. [b] Quadrupole splitting. [c] Line width. [d] Errors in the fitting results were noted in parentheses (Δk = 2-9 □$^{-1}$). [e] Coordination number. [f] Distance between absorber and

backscattering atoms. [g] Debye-Waller factor. [h] CN_{Fe-N} and CN_{Fe-O} were fixed to 4 and 1, respectively, on the basis of i) our previous XANES-EXAFS structure identification of FeN_xC_y moieties[7] and ii) Mössbauer spectroscopy showing that 95 % Fe in FeNC-1 is present as FeN_4 moieties. The EXAFS fitting was carried out with Fe-N, Fe-O and Fe-Fe bond distances and CN_{Fe-Fe} as variables. [i] CN_{Fe-Fe} of 0.6 corresponds well with the value of 0.64 which is calculated for FeNC-1 from the knowledge of i) the relative Fe-content of α-Fe and γ-Fe determined by Mössbauer spectroscopy and ii) known CN_{Fe-Fe} in pure α-Fe and γ-Fe. However, it cannot be excluded that a small fraction of the Fe-Fe EXAFS signal for FeNC-1 originates from binuclear $Fe_2N_xC_y$ sites that were recently suggested by Holby *et al.*[14,15] (see also Fig. S1f and its caption).

References

1. G. Wu, K. Artyushkova, M. Ferrandon, J. Kropf, D. Myers and P. Zelenay, *E CS Trans.*, 2009, **25**, 1299-1311.
2. B. Ravel and M. Newville, *J. Synchrotron Radiat.*, 2005, **12**, 537-541.
3. H. C. Du, *Ultramicroscopy*, 2015, **151**, 62-67.
4. D. Guo, R. Shibuya, C. Akiba, S. Saji, T. Kondo and J. Nakamura, *Science*, 2 016, **351**, 361-365.
5. J. Zhang, X. Liu, R. Blume, A. Zhang, R. Schlögl and S. S. Dang, *Science*, 2 008, **322**, 73-77.
6. A. Bagri, C. Mattevi, M. Acik, Y. J. Chabal, M. Chhowalla and V. B. Shenoy , *Nat. Chem.*, 2010, **2**, 581-587.
7. A. Zitolo, V. Goellner, V. Armel, M. T. Sougrati, T. Mineva, L. Stievano, E. Fonda and F. Jaouen, *Nat. Mater.*, 2015, **14**, 937-942.
8. J. Herranz, F. Jaouen, M. Lefèvre, U. I. Kramm, E. Proietti, J. P. Dodelet, P. Bogdanoff, S. Fiechter, I. Abs-Wurmbach, P. Bertrand, T. M. Arruda and S. M ukerjee, *J. Phys. Chem. C*, 2011, **115**, 16087-16097.
9. H. L. Guo, X. F. Wang, Q. Y. Qian, F. B. Wang and X. H. Xia, *ACS Nano*, 2009, **3**, 2653-2659.
10. S. Y. Toh, K. S. Loh, S. K. Kamarudin and W. R. W. Daud, *Chem. Eng. J.*, 2014, **251**, 422-434.
11. G. Kresse and J. Furthmüller, *Comp. Mater. Sci.*, 1996, **6**, 15-50.
12. B. Hammer, L. B. Hansen and J. K. Nørskov, *Phys. Rev. B*, 1999, **59**, 7413-7 421.

13. M. Fishman, H. L. Zhuang, K. Mathew, W. Dirschka and R. G. Hennig, *Phys. Rev. B*, 2013, **87**, 245402.

14. E. F. Holby and C. D. Taylor, *Sci. Rep.*, 2015, **5**, 9286.

15. E. F. Holby, G. Wu, P. Zelenay and C. D. Taylor, *J. Phys. Chem. C*, 2014, **1 18**, 14388-14393.

16. S. Kattel and G. Wang, *J. Phys. Chem. Lett.*, 2014, **5**, 452-456.

17. S. Fletcher, *J. Solid State Electrochem.*, 2009, **13**, 537-549.

18. Z. Duan and G. Wang, *Phys. Chem. Chem. Phys.*, 2011, **13**, 20178-20187.